Contribution from the Department of Inorganic Chemistry,
University of Newcastle upon Tyne, NE1 7RU, England

Crystal Structure of Bis[μ-bis(trifluoromethyl)phosphido]-tetranitrosyldiiron, $Fe_2(NO)_4[\mu\text{-}P(CF_3)_2]_2$

WILLIAM CLEGG

Received April 26, 1976 AIC60297J

Bis[μ-bis(trifluoromethyl)phosphido]-tetranitrosyldiiron crystallizes in the triclinic space group $P\bar{1}$, with a = 7.294 (1), b = 7.492 (1), c = 8.147 (2) Å, α = 81.18 (2), β = 73.49 (2), γ = 84.77 (2)°. The structure has been determined from 2156 x-ray counter intensities by Patterson and Fourier techniques and refined by full-matrix least-squares methods to R = 5.19% (4.75% weighted). The unit cell contains one centrosymmetric molecule with a planar Fe_2P_2 ring. Principal geometrical parameters are Fe–P = 2.205 (1) Å, Fe–Fe = 2.747 (1) Å, and Fe–P–Fe = 77.1 (1)°. Available structural data for related complexes are summarized and compared with corresponding bridged carbonyl dimers.

Introduction

We have previously reported[1] the crystal structure of $Fe_2(CO)_6[\mu\text{-}P(CF_3)_2]_2$, a dimeric carbonyl complex with phosphido bridges having strongly electron-withdrawing CF_3 substituents. We concluded from the observed structure, together with qualitative isovalent hybridization arguments and simple extended Hückel-type molecular orbital calculations,[2] that the length and strength of the formal metal–metal single bond in such $Fe_2(CO)_6(\mu\text{-}B)_2$ complexes was secondary to the metal-bridge bonding and the electronic effects of the bridging ligands. We now report the crystal structure of the corresponding dimeric nitrosyl complex, $Fe_2(NO)_4[\mu\text{-}P(CF_3)_2]_2$,[3] which we compare with available structural data for related complexes.

Experimental Section

Crystal Data. $[Fe(NO)_2P(CF_3)_2]_2$, M = 569.7, triclinic, a = 7.294 (1), b = 7.492 (1), c = 8.147 (2) Å, α = 81.18 (2), β = 73.49 (2), γ = 84.77 (2)°, U = 421.2 Å,[3] d_{calcd} = 2.246, $d_{measured}$ = 2.21 g cm^{-3}, Z = 1, $F(000)$ = 274. Space group $P\bar{1}$. Mo $K\alpha$ radiation, Zr filtered, λ 0.710 69 Å, μ(Mo Kα) = 21.15 cm^{-1}.

Data Collection and Reduction. The black crystals were parallelepipeds with faces parallel to the unit cell faces. Initial values for the cell parameters were obtained by a least-squares refinement based on the observed and calculated positions of spots on ($hk0$), ($h0l$), and ($0kl$) precession photographs (Mo Kα radiation). The unit cell corresponds to the positive (type I) reduced form.[4] There were no systematic absences; possible space groups are $P1$ (No. 1) or $P\bar{1}$ (No. 2). The density was measured by flotation in bromoform–tetrachloroethylene.

A crystal of dimensions 0.085 × 0.280 × 0.490 mm (perpendicular distances between faces 100 and $\bar{1}00$, 010 and $0\bar{1}0$, 001 and $00\bar{1}$, measured with a travelling microscope) was sealed in a thin-walled Lindemann glass capillary and mounted on a Hilger and Watts Y290 diffractometer, with the c axis misaligned about 10° from the instrument ϕ axis; crystals mounted on glass fibers and exposed to the atmosphere had been found to decompose rapidly in the x-ray beam. The unit cell parameters and orientation matrix were obtained by a least-squares refinement[5] based on the automatically determined setting angles at room temperature of twelve reflections with 2θ between 35° and 50°.

The intensities of all independent reflections with $2\theta < 60°$ were measured at room temperature in the θ–2θ scan mode. Each reflection was scanned by 80 steps of 0.01° in θ, with a 3 s count at each step and a 60 s background count at each end of the scanning range. Calibrated attenuators were inserted for very intense reflections.

Three standard reflections measured after every 40 reflections showed a steady decline in intensity, the total decay being 11.3, 9.9, and 9.4%. Linear decay functions were fitted to the measurements and the average used to bring all the intensities to a common scale.[6]

Intensities and their estimated standard deviations were calculated as reported previously,[1] with a value of 0.05 for the "instability factor" P. Absorption corrections were applied by a Gaussian integration method; transmission factors range from 0.547 to 0.828. All reflections with positive recorded intensity were used in structure solution and refinement; the number of independent reflections was 2156.

The centrosymmetric space group $P\bar{1}$ was indicated by the statistical distribution of E values and was confirmed by successful solution and refinement of the structure. This requires the molecule itself to have a center of symmetry, with the Fe_2P_2 ring planar.

Structure Solution and Refinement. The iron and phosphorus atoms were located by interpretation of a Patterson synthesis and used to phase a Fourier synthesis, which revealed the positions of all the other atoms. Positional and thermal parameters were refined by full-matrix least-squares methods; the quantity minimized was $\sum w\Delta^2$, with $w = 1/\sigma^2(F_o)$ and $\Delta = |F_o| - |F_c|$. Atomic scattering factors for uncharged atoms, including corrections for anomalous scattering, were taken from ref 7.

Two cycles of refinement with isotropic thermal parameters for all atoms gave values for R ($=\sum|\Delta|/\sum|F_o|$) and R_w ($=\{\sum w\Delta^2/\sum wF_o^2\}^{1/2}$) of 14.0 and 12.7%, respectively. With the introduction of anisotropic thermal parameters for all atoms, refinement converged after several more cycles, giving R = 5.19% and R_w = 4.75%. The largest shift/esd ratio for the atomic coordinates in the last cycle was 0.012 and, for the thermal parameters, 0.005. The final value of S ($=\{\sum w\Delta^2/[N-P]\}^{1/2}$ for N reflections and P refined parameters) was 1.21; the rms deviation of a reflection of unit weight on an absolute scale of F_c ($=\{\sum w\Delta^2/\sum w\}^{1/2}$) was 0.49 electron and showed no systematic trends with indices, sin θ or F_o. The weighting scheme was thus shown to be consistent.[8] No significant extinction effects were indicated by a comparison of F_o and F_c for strong, low-angle reflections, so no corrections were applied. A final difference synthesis showed no peaks higher than 0.8 e Å^{-3}, the largest being close to the heaviest atoms, and no depressions lower than −0.4 e Å^{-3}.

Observed and calculated structure factors on a 10× absolute scale (electrons) are tabulated as supplementary material [see the final paragraph of this paper for details]. Positional and thermal parameters are given in Table I, interatomic distances and bond angles in Table II, and selected least-squares planes fitted to atomic positions in Table III.

Results

The molecular structure is shown in Figure 1. The view direction is chosen to demonstrate the relationship between this molecule and $Fe_2(CO)_6[\mu\text{-}P(CF_3)_2]_2$.[1] The molecule has crystallographic $\bar{1}$ (C_i) symmetry and approximate mmm (D_{2h}) symmetry, as is illustrated by the atom deviations and dihedral angles in Table III. The central Fe_2P_2 ring is planar (a requirement of the space group symmetry). A similar geometry has been observed in the related complexes $Fe_2(NO)_4(\mu\text{-}SEt)_2$,[9] $Fe_2(NO)_4(\mu\text{-}I)_2$,[10] and $Ni_2(CO)_4(\mu\text{-}PPh_2)_2$,[11] and the main geometrical features of these complexes are compared in Table IV.

The coordination about the iron atoms may be described as distorted tetrahedral, the N–Fe–N angle being opened up and the P–Fe–P angle reduced from 109.5°. The formal Fe–Fe single bond (required by "electron counting" and the observed diamagnetism) is considered not to occupy a discrete coordination site in this description.[3] Unlike the case of the dimeric carbonyl compounds $Fe_2(CO)_6(\mu\text{-}B)_2$,[12] the Fe–Fe bond in the nitrosyl is undoubtedly linear.

The Fe–N–O groups are slightly bent toward each other; the O···Fe···O angle is 4.4° smaller than N–Fe–N and the O–N–Fe–N torsion angles[13] τ (seen in Newman projections along the N–Fe bonds as in **1**) are −21 and 5°. The degree

Table I. Atomic Coordinates ($\times 10^4$)[a] and Anisotropic Thermal Parameters ($Å^2 \times 10^4$)[a,b]

Atom	x	y	z	U_{11}	U_{22}	U_{33}	U_{23}	U_{13}	U_{12}
Fe	−399.6 (6)	1502.5 (5)	842.8 (5)	497 (3)	405 (2)	330 (2)	−18 (1)	−127 (2)	26 (2)
P	−308.6 (10)	1300.6 (9)	−1850.5 (9)	449 (4)	421 (4)	320 (4)	36 (3)	−124 (3)	−13 (3)
N(1)	1419 (4)	2753 (4)	706 (4)	672 (18)	480 (14)	537 (16)	−96 (12)	−192 (14)	−36 (12)
O(1)	2594 (5)	3725 (4)	634 (5)	951 (23)	814 (20)	1151 (27)	−202 (18)	−364 (20)	−314 (17)
N(2)	−2636 (4)	2069 (4)	1857 (4)	578 (17)	679 (18)	449 (15)	−71 (13)	−119 (13)	97 (13)
O(2)	−4139 (5)	2604 (5)	2584 (5)	694 (19)	1327 (29)	908 (24)	−249 (21)	21 (17)	319 (18)
C(1)	1477 (5)	2679 (5)	−3585 (4)	552 (18)	622 (19)	449 (18)	82 (15)	−134 (14)	−42 (14)
F(11)	1435 (4)	2499 (4)	−5165 (3)	1008 (18)	1065 (18)	354 (11)	47 (11)	−61 (11)	−180 (14)
F(12)	1158 (4)	4436 (3)	−3475 (3)	1129 (20)	586 (13)	843 (18)	66 (12)	−10 (15)	−266 (12)
F(13)	3195 (3)	2214 (4)	−3449 (4)	464 (12)	1512 (25)	1020 (21)	510 (18)	−169 (13)	−162 (13)
C(2)	−2517 (5)	1861 (4)	−2593 (4)	545 (18)	529 (17)	459 (17)	16 (13)	−208 (14)	−20 (13)
F(21)	−2996 (4)	3595 (3)	−2755 (4)	868 (16)	588 (12)	1286 (22)	−28 (13)	−614 (16)	160 (11)
F(22)	−2371 (4)	1346 (4)	−4094 (3)	944 (18)	1385 (23)	753 (17)	−404 (16)	−517 (14)	203 (16)
F(23)	−3961 (3)	1034 (4)	−1478 (4)	562 (13)	1263 (21)	1008 (20)	428 (17)	−294 (13)	−281 (13)

[a] In this and subsequent tables, estimated standard deviations in the last place of figures are given in parentheses. [b] The anisotropic temperature factor takes the form $\exp[-2\pi^2(h^2a^{*2}U_{11} + \ldots + 2hka^*b^*U_{12} + \ldots)]$.

Table II. Bond Lengths (Å) and Bond Angles (deg)

Fe-P	2.204 (1)	P-C(1)	1.874 (3)
Fe-P′[a]	2.206 (1)	P-C(2)	1.868 (3)
Fe-Fe′	2.747 (1)	C(1)-F(11)	1.324 (4)
Fe-N(1)	1.661 (3)	C(1)-F(12)	1.328 (4)
Fe-N(2)	1.655 (3)	C(1)-F(13)	1.301 (4)
N(1)-O(1)	1.158 (4)	C(2)-F(21)	1.310 (3)
N(2)-O(2)	1.156 (4)	C(2)-F(22)	1.311 (4)
		C(2)-F(23)	1.312 (4)
Fe′-Fe-P	51.5 (1)	Fe′-P-C(1)	121.8 (1)
Fe′-Fe-P′	51.4 (1)	Fe′-P-C(2)	120.6 (1)
Fe′-Fe-N(1)	117.4 (1)	C(1)-P-C(2)	101.1 (1)
Fe′-Fe-N(2)	120.2 (1)	P-C(1)-F(11)	113.3 (2)
P-Fe-P′	102.9 (1)	P-C(1)-F(12)	111.7 (2)
P-Fe-N(1)	105.3 (1)	P-C(1)-F(13)	109.7 (2)
P-Fe-N(2)	107.4 (1)	F(11)-C(1)-F(12)	105.3 (3)
P′-Fe-N(1)	108.1 (1)	F(11)-C(1)-F(13)	108.3 (3)
P′-Fe-N(2)	109.1 (1)	F(12)-C(1)-F(13)	108.2 (3)
N(1)-Fe-N(2)	122.4 (1)	P-C(2)-F(21)	113.5 (2)
Fe-N(1)-O(1)	175.2 (3)	P-C(2)-F(22)	113.2 (2)
Fe-N(2)-O(2)	174.0 (3)	P-C(2)-F(23)	109.5 (2)
Fe-P-Fe′	77.1 (1)	F(21)-C(2)-F(22)	105.9 (3)
Fe-P-C(1)	116.8 (1)	F(21)-C(2)-F(23)	107.6 (3)
Fe-P-C(2)	119.8 (1)	F(22)-C(2)-F(23)	106.8 (3)
		O(1)...Fe...O(2)	118.0 (1)

Intermolecular Distances Less Than 3.3 Å

Atoms	Distance, Å	Transformation[b]
O(2)...O(1)	3.207	$-1+x, y, z$
F(11)...O(1)	3.287	$x, y, -1+z$
F(21)...O(1)	2.926	$-x, 1-y, -z$
F(11)...O(2)	3.230	$1+x, y, -1+z$
F(13)...O(2)	3.249	$1+x, y, -1+z$
F(22)...O(2)	3.295	$x, y, -1+z$
F(12)...F(11)	3.114	$-x, 1-y, -1-z$
F(21)...F(11)	3.275	$-x, 1-y, -1-z$
F(22)...F(11)	3.011	$-x, -y, -1-z$
F(21)...F(12)	3.169	$-x, 1-y, -1-z$
F(21)...F(13)	3.271	$-1+x, y, z$
F(22)...F(13)	3.148	$-1+x, y, z$
F(23)...F(13)	2.964	$-1+x, y, z$

[a] The prime indicates an atom related by inversion through the center of symmetry at the unit cell origin. [b] The distances given are between the first atom in one molecule and the second atom in another molecule related by the symmetry transformations shown.

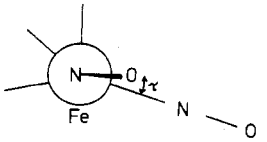

1

and direction of bending are consistent with the calculations of Summerville and Hoffmann[14] on $(ON)_2ML_2$ complexes.

Table III. Least-Squares Planes[a] in Terms of Orthogonal Ångström Axes along a*, c × a*, and c

A. Equations of Planes

(1) $0.9712X + 0.2381Y + 0.0122Z = 0$
(2) $0.1308X - 0.5306Y + 0.8375Z = 0$
(3) $-0.2329X + 0.7824Y + 0.5777Z = 0$

B. Deviations ($Å \times 10^3$) of Atoms from the Planes

Atom[b]	Δ_1	Δ_2	Δ_3
Fe	0	31	
P	0		−27
N(1)		15	
O(1)		−33	
N(2)		4	
O(2)		−29	
C(1)			19
C(2)			20
Rms deviation	0	27	24

C. Dihedral Angles (deg) between Planes

(1)-(2)	89.4
(1)-(3)	91.9
(2)-(3)	87.8

[a] Atoms were assigned weights for the calculation proportional to the atomic numbers. [b] For each atom, the centrosymmetrically related atom was also included in the calculation. Thus, all three planes intersect at the unit cell origin, and the deviations for related atoms are equal and opposite in sign.

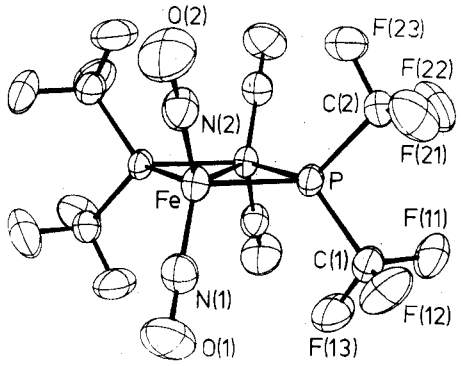

Figure 1. Perspective view showing thermal motion as 40% probability contours.

The Fe–N and N–O bond lengths are typical of iron nitrosyl complexes.

The crystal packing is shown in Figure 2, by a projection along the crystallographic x axis. There are no unusual intermolecular interactions (see Table II) and no unusual thermal parameters (see Table I and Figure 1); CF_3 torsional vibration, while significant, is considerably less than that found for two of the CF_3 groups in $Fe_2(CO)_6[\mu\text{-}P(CF_3)_2]_2$.[1]

Table IV. $M_2L_4(\mu\text{-}B)_2$ Complexes (Bond Lengths (Å) and Angles (deg))

Complex	M-B	M-M	M-B-M	B-M-B	L-M-L
$Fe_2(NO)_4(\mu\text{-}I)_2$[a,b]	2.570 (4)	3.013 (7)	71.8 (1)	108.2 (1)	117.8 (12)
	2.582 (4)	3.089 (7)	73.4 (1)	106.6 (1)	115.0 (13)
$Fe_2(NO)_4(\mu\text{-}SEt)_2$[c]	2.270 (4)	2.720 (3)	74.0 (1)	106.0 (1)	117.4 (2)
$Fe_2(NO)_4[\mu\text{-}P(CF_3)_2]_2$[d]	2.205 (1)	2.747 (1)	77.1 (1)	102.9 (1)	122.4 (1)
$Ni_2(CO)_4(\mu\text{-}PPh_2)_2$[a,e]	2.190 (3)	2.515 (2)	70.1 (1)	109.9 (1)	115.9 (4)
	2.194 (3)	2.505 (1)	69.6 (1)	110.4 (1)	118.2 (5)

[a] There are two crystallographically independent molecules in the unit cell. [b] Reference 10. [c] Reference 9. [d] This work. [e] Reference 11.

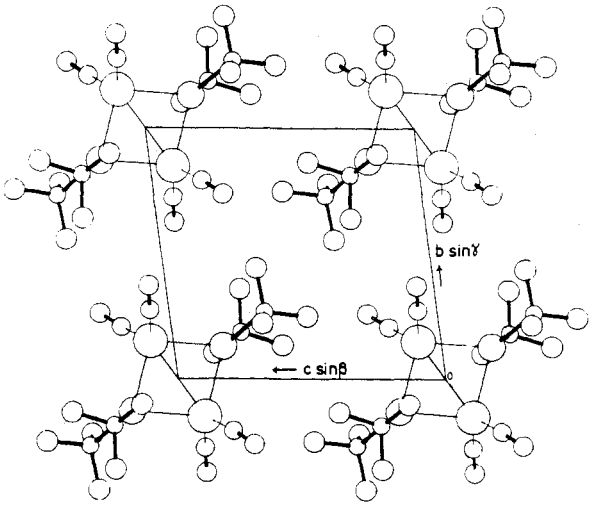

Figure 2. Projection along the *x* axis.

Discussion

In our discussion of the dimeric carbonyl complexes,[1,2] we considered the "flap angle" between the two FeB_2 planes of the folded central Fe_2B_2 ring (**2**) to be of particular interest

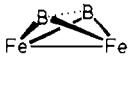

2

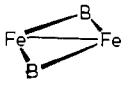

3

and diagnostic importance in understanding the bonding and geometry of the molecules. The use of an angle rather than a distance for measuring the bridging geometry facilitates the comparison of complexes containing different bridging atoms, when the Fe–B bond lengths vary over a large range and the Fe–Fe distances vary roughly in parallel with them. The dimeric iron nitrosyl complexes (and isoelectronic nickel carbonyl complex) in Table IV have a planar central ring with a flap angle of 180° (**3**). For an idealized D_{2h} (*mmm*) symmetry of the central ring **3**, only two parameters are required to describe the geometry, compared with three for the idealized C_{2v} (*mm*2) folded ring **2**: either two distances (e.g., Fe–B and Fe–Fe) or one distance and one angle (e.g., Fe–B and Fe–B–Fe). We concentrate here on the second description, using the Fe–B–Fe angle rather than the Fe–Fe distance as a measure of the bridging geometry, allowing us to compare on one scale structures containing different bridging ligands. Thus, for the four complexes in Table IV, the M–B distances cover a range of nearly 0.4 Å, and the M–M distances cover more than 0.5 Å, but the internal angles of the ring vary by only 7.5°; the range of L–M–L angles is similar.

Such an acute M–B–M angle has previously been interpreted[10,11,15] in terms of a significant direct metal–metal bonding interaction across the ring, pulling the metal atoms together. In their recent detailed theoretical study of $M_2L_4(\mu\text{-}B)_2$ dimers,[14] Summerville and Hoffmann incline rather to the view that, in the d^9 or $\{M(NO)_2\}^9$ case,[16] the bridging geometry reflects the geometrical preference of the ML_2B_2 distorted tetrahedral monomer, with little evidence for direct metal–metal σ bonding. It was possible to assess in a simple way[1,2] the relative importance of M–B and M–M interactions in determining the geometry of $Fe_2(CO)_6(\mu\text{-}B)_2$ complexes and to examine the effect of varying the electronegativity of the bridging ligand substituents, because the highest occupied molecular orbital (HOMO) for the system was energy and geometry determining to a large degree; the energy of the HOMO varied much more with flap angle than any other occupied MO. The situation is much less simple for the d^9 or $\{M(NO)_2\}^9$ dimers in Table IV. That no single occupied orbital dominates the system is clear in Summerville and Hoffmann's Figures 5 and 8, and calculations for the model complex $Fe_2(NO)_4(\mu\text{-}PF_2)_2$ give a similar picture.[17] In attempting to assess the effect of the strongly electron-withdrawing CF_3 groups on the geometry of the Fe_2P_2 ring in $Fe_2(NO)_4[\mu\text{-}P(CF_3)_2]_2$ we also have the problem, unlike the carbonyl case, of few other structures with which to make comparisons and, in particular, no other phosphido-bridged iron nitrosyl $Fe_2(NO)_4(\mu\text{-}PR_2)_2$. A simple isovalent hybridization argument[18] would lead us to expect, as in the dimeric carbonyl case,[1] a closing down of the $F_3C\text{–}P\text{–}CF_3$ angle and hence a wider Fe–P–Fe angle and longer Fe–Fe distance in the CF_3-substituted complex than in the CH_3-substituted analogue. A cursory glance at the M–B–M angles in Table IV might tend to strengthen this expectation; this angle is largest for the $[\mu\text{-}P(CF_3)_2]_2$ complex, the comparison with the nickel carbonyl complex, which has a phosphido bridge without strongly electron-withdrawing substituents, being particularly striking. However, the Fe–S–Fe angle in the $(\mu\text{-}SEt)_2$ complex is not much smaller, and this contrasts strongly with the carbonyl case.[14] Table V summarizes Fe–Fe distances and Fe–B–Fe angles for bridging ligands occurring in both the carbonyl and the nitrosyl series. The bridging angle is greater for the sulfur-bridged nitrosyl than for the corresponding carbonyl but smaller for the phosphorus-bridged nitrosyl than for the corresponding carbonyl. Without further structural data in the nitrosyl series, and without the assistance of a single dominant factor in the simple molecular orbital picture, we are unable at this stage to untangle the electronic effects of the substituents from the effect of substituting bridging phosphorus for bridging sulfur in the nitrosyl series. Research is in progress to obtain further data to resolve this problem.

Table V. Bridging Angles (deg) and Metal–Metal Distances (Å) in Related Complexes of the Carbonyl and Nitrosyl Series

	B = SEt[a]	B = PR_2[b]	B = $P(CF_3)_2$[c]
$Fe_2(CO)_6(\mu\text{-}B)_2$	68.3 (3)	72.0–74.2 (1)	80.0 (1)
	2.537 (10)	2.619–2.665 (2)	2.819 (1)
$Fe_2(NO)_4(\mu\text{-}B)_2$	74.0 (1)		77.1 (1)
	2.720 (4)		2.747 (1)

[a] References 9 and 15. [b] References 1 and 19. [c] Reference 1 and this work.

Acknowledgment. I wish to thank Dr. R. C. Dobbie for providing crystals and Dr. H. M. M. Shearer for assistance

in the data collection at Durham University. Calculations were performed on the IBM 370/168 and Hewlett-Packard 2000E computers at Newcastle University. I am grateful to Dr. J. K. Burdett for his interest and for the use of his molecular orbital calculations.

Registry No. $[Fe(NO)_2P(CF_3)_2]_2$, 36486-27-8.

Supplementary Material Available: A listing of observed and calculated structure factor amplitudes (13 pages). Ordering information is given on any current masthead page.

References and Notes

(1) W. Clegg, *Inorg. Chem.*, **15**, 1609 (1976).
(2) J. K. Burdett, *J. Chem. Soc., Dalton Trans.*, in press.
(3) R. C. Dobbie, M. J. Hopkinson, and D. Whittaker, *J. Chem. Soc., Dalton Trans.*, 1030 (1972).
(4) A. D. Mighell, A. Santoro, and J. D. H. Donnay, "International Tables for X-ray Crystallography", Vol. 1, Kynoch Press, Birmingham, England, 1974, p 530.
(5) W. R. Busing and H. A. Levy, *Acta Crystallogr.*, **22**, 457 (1967).
(6) Computer programs used in this study, other than those of the author, were local versions of the following: for crystal structure determination and refinement, SHEL-X (G. M. Sheldrick, Cambridge, England); for least-squares planes, XANADU (G. M. Sheldrick and P. J. Roberts, Cambridge, England); for Figure 1, ORTEP (C. K. Johnson, Oak Ridge, Tenn.); for Figure 2, PLUTO (W. D. S. Motherwell, Cambridge).
(7) D. T. Cromer and J. T. Waber, ref 4, Vol. IV, p 99; D. T. Cromer and J. A. Ibers, *ibid.*, p 149.
(8) W. C. Hamilton, ref 4, Vol. IV, p 293.
(9) J. T. Thomas, J. H. Robertson, and E. G. Cox, *Acta Crystallogr.*, **11**, 599 (1958).
(10) L. F. Dahl, E. R. de Gil, and R. D. Feltham, *J. Am. Chem. Soc.*, **91**, 1653 (1969).
(11) J. A. J. Jarvis, R. H. B. Mais, P. G. Owston, and D. T. Thompson, *J. Chem. Soc. A*, 1867 (1970).
(12) B. K. Teo, M. B. Hall, R. F. Fenske, and L. F. Dahl, *Inorg. Chem.*, **14**, 3103 (1975).
(13) F. H. Allen and D. Rogers, *Acta Crystallogr., Sect. B*, **25**, 1326 (1969).
(14) R. H. Summerville and R. Hoffmann, *J. Am. Chem. Soc.*, in press.
(15) L. F. Dahl and C.-H. Wei, *Inorg. Chem.*, **2**, 328 (1963).
(16) The notation $\{M(NO)_x\}^n$ is that of J. H. Enemark and R. D. Feltham. *Coord. Chem. Rev.*, **13**, 339 (1974).
(17) J. K. Burdett, unpublished results.
(18) R. S. Mulliken, *J. Phys. Chem.*, **41**, 318 (1937); **56**, 295 (1952); H. A. Bent, *J. Chem. Phys.*, **33**, 1259 (1960).
(19) J. R. Huntsman and L. F. Dahl, to be published.

Notes

Contribution from the Department of Chemistry, Université de Montréal, Montréal, Québec, Canada

Preparation of Finely Divided VCl_3 by Decomposition of VCl_4 in an Electrical Discharge

B. Fisa, J. F. Revol, and R. H. Marchessault*[1]

Received October 21, 1975 AIC50764H

Vanadium trichloride complexed with certain organometalic compounds is often used to promote various polymerization reactions. The activity of heterogeneous catalysts, such as VCl_3, is greatly influenced by their surface characteristics. High specific surface (hence small particle size) and irregularly shaped particles are desirable. This is achieved when crystals develop at high supersaturation, i.e., in conditions far from the crystallization equilibrium. Pure VCl_3 can be prepared by thermal decomposition[2] of VCl_4 at 150–170 °C. This reaction yields crystals larger than 10 μm^3. Since the solid-state texture of vanadium trichloride cannot be altered by the traditional postsynthesis treatments[4] it is desirable to devise reaction methods which yield smaller particles of VCl_3.

We have recently found that very finely divided VCl_3 is produced when VCl_4 vapors are excited in an electrical discharge

$$2VCl_4(g) \rightarrow 2VCl_3(s) + Cl_2(g)$$

Exploratory experiments have shown that this reaction is very fast; its rate in the discharge is many times higher than the rate of thermal decomposition of VCl_4 vapors observed in our laboratories.[5] Examination of the product in a transmission electron microscope revealed very small (~0.1 μm) round particles. Despite the small particle size, the discharge-made VCl_3 and the commercial VCl_3 (made by thermal decomposition of VCl_4) give the same x-ray powder diagram.

Although vanadium tetrachloride is an unstable compound and decomposes slowly to VCl_3, even at room temperature, the ease of decomposition in the discharge appears surprising in the light of known thermodynamic data. Heating of gaseous VCl_4 by the discharge energy accelerates the reaction, but as the temperature increases, the equilibrium shifts to the VCl_4 side. At 160 and 180 °C the equilibrium constant K_p ($P_{Cl_2}/P_{VCl_4}^2$) assumes the values of 6.8×10^{-4} and 3.3×10^{-4} (in $mmHg^{-1}$) respectively.[6] Since we have used pressures lower than 1 mmHg, very little VCl_4 should have decomposed if the transfer of thermal energy were the only important effect of the discharge. At low temperatures, when the equilibrium lies on the VCl_3 side,[7] the decomposition is very slow; at 20 °C liquid VCl_4 has a half-life of 4150 months.[8]

Formation of VCl_3 can be rationalized if one considers interaction of excited species with the reactor wall. If an excited molecule remains in the discharge zone without colliding with the reactor wall, probability of back-reaction is high.[9] On the other hand, when an excited molecule collides with and is absorbed on a cold reactor wall, equilibrium conditions favor the formation of VCl_3. This interpretation is also supported by differences in the behavior of VCl_4 and $TiCl_4$ in the discharge. Both can be reduced to their respective trichlorides by atomic hydrogen generated in the discharge[10,11] but all reported attempts to reduce titanium tetrachloride (which is thermodynamically stable[7]) in hydrogen-free discharges have failed.[11,12]

Experimental Section

VCl_4 (Stauffer; highest purity) was added to a round-bottom flask under an inert atmosphere. The flask was connected to a grease-free vacuum system; VCl_4 was cooled to about −20 °C and degassed for approximately 1 h by slow pumping. It was then cooled to liquid nitrogen temperature and the whole system was thoroughly evacuated (to 10^{-4} mmHg or less). The vanadium tetrachloride was then allowed to heat up and was distilled through a 700 mm long, 31-mm o.d. glass tube (made from Pyrex 7740). When radiofrequency power (5.2 MHz, 100 W, 2000 V) was applied using a coil applicator, a pale blue-green glow developed and VCl_3 started immediately to deposit on the tube walls. If the power was interrupted after a few seconds, a fine iridescent coating was obtained. After about 1 min the whole discharge tube was covered with an opaque purple layer of VCl_3. However, the discharge could be maintained despite the VCl_3 deposit. The pronounced color of VCl_4 vapors allowed an estimation of the pressure within the reaction tube. The best results were obtained when the pressure was between 0.1 and 1 mmHg. Alternatively, a Tesla coil could be used instead of a radiofrequency generator, if the discharge tube had a constriction (3–5 mm in diameter) and the discharge was applied at that point.

Acknowledgment. We appreciate support from the National Research Council of Canada.

Registry No. VCl_3, 7718-98-1; VCl_4, 7632-51-1.